

Crystal nucleation mechanism in melts of short polymer chains under quiescent conditions and under shear flow

Muhammad Anwar,¹ Joshua T Berryman,¹ and Tanja Schilling¹

Université du Luxembourg, Theory of Soft Condensed Matter Physics, Physics and Materials Research Unit, L-1511 Luxembourg, Luxembourg

(Dated: 16 August 2022)

We present a molecular dynamics simulation study of crystal nucleation from undercooled melts of *n*-alkanes, and we identify the molecular mechanism of homogeneous crystal nucleation under quiescent conditions and under shear flow. We compare results for *n*-eicosane(C20) and *n*-pentacontahexane(C150), i.e. one system below the entanglement length and one above. Under quiescent conditions, we observe that entanglement does not have an effect on the nucleation mechanism. For both chain lengths, the chains first align and then straighten locally. Then the local density increases and finally positional ordering sets in. At low shear rates the nucleation mechanism is the same as under quiescent conditions, while at high shear rates the chains align and straighten at the same time. We report on the effects of shear rate and temperature on the nucleation rates and estimate the critical shear rates, beyond which the nucleation rates increase with the shear rate. We show that the viscosity of the system is not affected by the crystalline nuclei.

When a liquid is cooled below its crystal-liquid coexistence temperature, crystallites are formed. The shapes, sizes and structures of these crystallites strongly influence the properties of the final material. Polymer melts often flow during processing. Flow modifies crystal nucleation and growth processes and hence affects the materials properties of crystalline and semicrystalline plastics. Thus crystallization in flowing polymer melts is clearly a topic of technological relevance, but it is also a challenging topic from the point of view of basic theoretical physics. Relaxation in polymer melts occurs on a hierarchy of time-scales that spans several orders of magnitude. When discussing phase transitions in polymers, one inevitably deals with non-equilibrium processes, which can only to a very limited extent be described by quasi-equilibrium approaches. This fact poses a serious challenge to any attempt to theoretically model polymer crystallization.

In spite of intensive research efforts since the early 1940s, the molecular mechanism of polymer crystallization is still not completely understood¹. Experimental research has been carried out using a wide range of techniques in order to understand the crystallization mechanism of polymers under quiescent conditions^{2–11} and in external fields^{12–19}. Crystallization rates and critical shear rates have been measured for different polymeric materials, the morphological features of the final crystal structure and the effect of molecular weight on the crystallization kinetics have been studied. But the primary nucleation mechanism has not been identified, because the short length- and time-scales on which it takes place are difficult to access.

Most theoretical approaches to flow induced crystallization are based on coarse-graining. Generally, sets of coupled differential equations for the time evolution of macroscopic quantities (such as e.g. the volume occupied by crystallites or the thickness of lamellae) are

derived partly from the underlying microscopic theories, partly from balance conditions and considerations regarding the structure of effective free energy landscapes (see e.g. refs. [16,20–27]). While undoubtedly useful, these models are inevitably semi-empirical. Coarse-graining requires approximations already in the equilibrium case. For the non-equilibrium case, in which one usually does not know the probability distributions of microstates according to which state-space averages would need to be taken, no systematic approach exists.

McLeish, Olmsted and co-workers have over the past 15 years developed a comprehensive set of theoretical and computer simulation techniques and experimental model systems to study polymers under flow. To address crystallization they derived a kinetic Monte Carlo algorithm on the basis of kinetics extracted from the GLaMM model²⁸, embedded it in a Brownian dynamics simulation^{29,30} and extended this approach by a fast nucleation algorithm to compute nucleation rates³¹. This model captures many features of flow induced crystallization, however, parts of it are based on an effective free energy picture i.e. on the assumption of separating relaxation time-scales and thus quasi-equilibrium.

As the molecular length- and time scales involved in nucleation and growth processes are below experimental resolution, atomistic computer simulations have been used to study polymer crystallization under quiescent conditions^{32–54} and under flow or large deformation^{55–63}. Most of these studies focus on the growth process rather than the nucleation process, because nucleation is by definition a rare event (an event that occurs on a time-scale much larger than the time-scale of the local dynamics) and therefore difficult to tackle by atomistic simulation. Nucleation in short chain alkanes under quiescent conditions has nevertheless been simulated^{32–37,39,40} and a scenario for the nucleation mechanism has been identified. (We will refer to this mechanism in detail in the

results section.) The first direct computation of homogeneous nucleation rates in long chain alkanes by means of computer simulation has recently been presented by Rutledge and co-workers³⁸. Their work was focussed on the nucleation and growth rates and the free energy landscape associated with the crystallization process rather than the microscopic mechanisms.

To our knowledge, there is no simulation study yet that resolves the molecular nucleation mechanism in polymers under shear. In this article, we present a detailed analysis of the formation of crystal nuclei from the melt in short chain alkanes under shear and in long chain alkanes under quiescent and shear conditions.

I. MODEL & ORDER PARAMETERS

We have used a united atom model for polyethylene that has been proposed by Paul et al.⁶⁴ and later modified by Waheed et al.⁵¹. (For a table of interaction parameters we refer the readers to our previous work⁴⁰.) In order to carry out the simulations by means of the ESPResSo package⁶⁵ we implemented (and have made available) the dihedral-cosine potential and Lees Edwards periodic boundary conditions, which were not previously supported by ESPResSo.

We used several order parameters to identify the crystallites in the melt: for the analysis we split the long chains (C150) into segments of 15 monomers, while we regarded the short chains (C20) as single segments. Then we computed the radius of gyration R_g of each segment and the nematic order parameter S_2 of those segments that were involved in the formation of the critical nucleus. (A definition and detailed description of these parameters can be found in our previous work on C20⁴⁰.) Further we measured the local alignment of bonds: Monomers within a radius $r_c = 1.4\sigma$ were considered as neighbours, where σ is the length scale set by the Lennard Jones interaction in the polymer model. Two neighbours i and j were considered as “aligned” if the chains they belonged to locally were almost parallel ($\theta_{ij} \leq 10^\circ$). For a particle to be considered “crystalline”, it had to have at least 13 aligned neighbours in case of C20 and 12 aligned neighbours in case of C150. These numbers were obtained by sampling the probability distributions of the number of aligned neighbours in the bulk crystal and the bulk liquid.

II. MOLECULAR DYNAMICS SIMULATIONS OF C150 UNDER QUIESCENT CONDITIONS

A. Simulation details

First we discuss the nucleation mechanism in a quiescent system of n -pentacontane (C150). We chose

TABLE I. Results of the mean first passage time analysis for C150 at 280 K.

System	n^*	t^* (ns)	$I(10^{25} \text{cm}^{-3} \text{s}^{-1})$
Yi et al. ³⁸	143 ± 14	293 ± 19	1.47 ± 0.10
This work	87 ± 9	354 ± 41	0.72 ± 0.08

C150, because it has the minimum length for which we can capture the effects of entanglement on crystallization and observe a folded chain crystal structure (the entanglement length has been reported to be between 60 and 90 monomers^{66–69}). We simulated 100 chains at 280K, which corresponds to 30% supercooling. (For the model that we use, the equilibrium melting temperature of C150 is 396.4K³⁸.) We equilibrated the system at 500K, i.e. well above the melting temperature. After equilibration we quenched the configurations from 500K to 280K and observed the nucleation event. We performed these simulations under constant pressure and constant temperature conditions. The pressure was fixed at 1 atmospheric pressure.

The polymer model contains a Lennard-Jones-type interaction term. We therefore use Lennard Jones units to present our data (i.e. the particle mass m , the interaction energy ϵ and resulting timescale $\tau = \sqrt{m\sigma^2/k_B T}$). Quantities which can be compared directly with the experimental results are presented in SI units. We used a Langevin dynamics based thermostat and barostat⁷⁰. The friction coefficient γ used for the thermostat was $1.0\tau^{-1}$ and the piston mass for the barostat was $0.00001m$.

B. Nucleus formation

To determine the induction time and the size of the critical nucleus we performed a mean first passage time analysis⁷¹ on 20 independent trajectories. (This method has been successfully applied to simulation data of nucleation in n -alkanes before^{36–38}.) The values for the induction time t^* and the number of particles in the critical nucleus n^* are given in Table I. We find the induction time to be in agreement with the results of Yi et al³⁸. The difference in the critical nucleus sizes is due to different criteria for identification of crystalline particles.

To analyze the nucleation mechanism, we identify in each trajectory those particles that are part of the critical nucleus at the nucleation time t_0 . We then trace them backwards in time and compute their structural and orientational properties. We proceed backwards until the particles are indistinguishable from the melt particles. For 20 independent trajectories we compute the average radius of gyration R_g of all chain segments that are part of the nucleus at t_0 , the nematic order S_2 of these chain segments, the average volume V of the Voronoi⁷² cell associated to each particle that is part of the nucleus and its crystallinity order parameter.

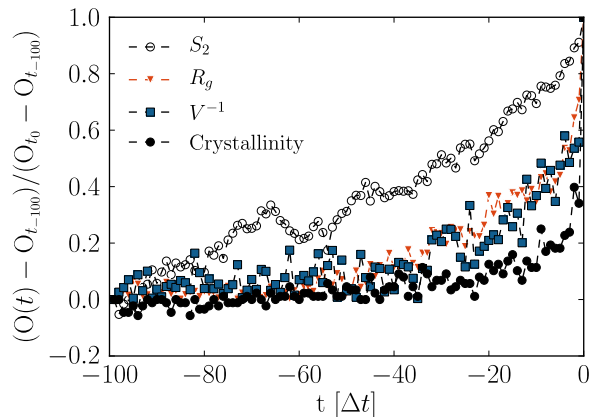


FIG. 1. Relative variation of several observables (O) from the melt to the formation of a critical nucleus, computed for the particles that are part of the nucleus: the orientational order parameter S_2 (black, open circles), the radius of gyration R_g (red, triangles), the inverse of the Voronoi cell volume V (blue, squares) and the crystallinity order parameter (black, closed circles). The curves are averaged over 20 independent trajectories progressing backward in time from the nucleation time $t = t_0$ in steps $\Delta t = 100000\tau$ to $t = -100\Delta t$.

In Fig. 1 we show the relative variations of these quantities with respect to the values they had at $-100\Delta t$, where $\Delta t = 100000\tau$. When we advance from the supercooled melt towards the formation of the critical nucleus at t_0 , we observe first an increase in the global orientational order S_2 , then an increase in the radius of gyration of the segments and in the local density, and finally the crystal structure is formed. We conclude that the nucleation mechanism in long, entangled chains is the same as in short, non-entangled chains: orientational ordering precedes straightening⁴⁰.

Note that the Voronoi volume per particle in the nucleus does not deviate from its melt value until the very late stages of the nucleation process. We are thus not dealing with the spinodal decomposition assisted crystallization process that has been proposed by Olmsted²⁵.

Doi et al. suggested that crystallization was initiated by an increase in the persistence length, followed by the alignment of the chains^{23,24}. Our results stand in contrast to this scenario, too.

In Fig. 2 we present snapshots of the formation of the critical nucleus at different times from $t = t_{-100}$ to $t = t_0$. The monomers that form the critical nucleus at t_0 are highlighted as large gray beads. The red color shows the segments of chains that participate with a single stem in the formation of the critical nucleus while blue, green and orange indicate those chains which fold back and participate in the formation of critical nucleus with more than one stem. For the case of folded chains we show complete chains instead of segments so that folds and

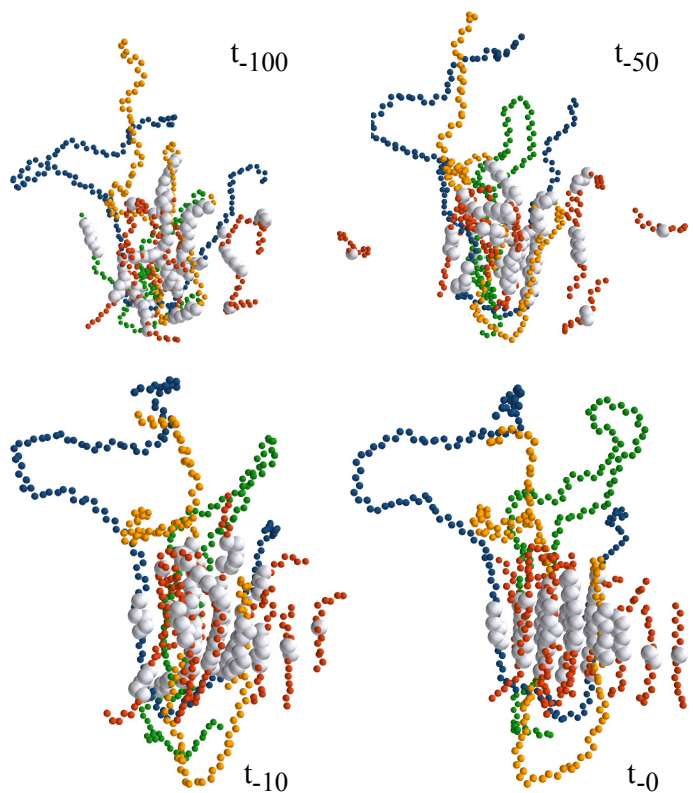


FIG. 2. Snapshots illustrating the nucleation mechanism. Large gray beads: monomers that form the critical nucleus at t_0 . Red: segments of chains that participate with a single stem in the formation of the critical nucleus. Blue, green and orange: chains which fold back and participate in the formation of critical nucleus with more than one stem. For the case of folded chains we show complete chains instead of segments so that folds and tails can be identified.

tails can be identified. The images of the formation of the nucleus are consistent with the mechanism we proposed based on the values of S_2 , R_g , V and the crystallinity order parameter (fig. 1).

The critical nuclei consist of some chain segment(stems) from different chains and some from the same chain, which is folded. The primary nucleation mechanism is thus a combination of intramolecular and intermolecular mechanisms. Fig. 3 shows the ratio of the number of stems to the number of chains. It is always larger than unity, i.e. there are folded and non-folded chains in the clusters.

III. MOLECULAR DYNAMICS SIMULATIONS OF C20 UNDER SHEAR

A. Simulation details

We studied the effect of shear on the nucleation rate and mechanism in n -eicosane (C20) by means of MD

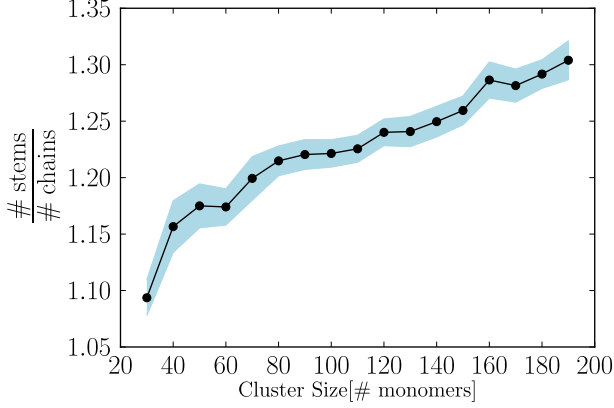


FIG. 3. Ratio of the number of stems to the number of chains against cluster size. The black curve (circles) shows the mean value and the light blue envelop shows the standard deviation.

simulations at controlled temperature and constant volume, particle number and shear rate in a box with Lees-Edwards boundary conditions. The system consisted of 500 chains. We equilibrated it at 450K, which is well above the melting temperature. (The equilibrium melting temperature of C20 in the simulation model we use is $310 \pm 2\text{K}$ ³⁷, which is in agreement with the experimentally observed value). To set the density of the metastable melt at 1 atm pressure we used Table II.

We quenched the system from 450K to 250K, applied shear and observed the nucleation event. We ran simulations at seven different shear rates ranging from $\dot{\gamma} = 0.000001\tau^{-1}$ to $\dot{\gamma} = 0.01\tau^{-1}$ ($0.95 \times 10^{10}\text{sec}^{-1}$ to $0.95 \times 10^6\text{sec}^{-1}$). We also performed simulations at zero shear rate for comparison and we did not find any difference between the nucleation rate at the lowest non-zero shear rate and at zero shear rate. We used the DPD thermostat⁷³ with the friction coefficient $\gamma_{\text{DPD}} 1.0\tau^{-1}$.

In order to avoid the artefactual decoupling of the system from its periodic images remarked upon by Chatterjee⁷⁴ when using the DPD thermostat to treat a dissipative shear-flow, a modification to the pairwise dissipative DPD force \vec{F}_{ij}^D was made:

$$\vec{v}_{ij}^{*\alpha} = \vec{v}_{ij}^{\alpha} - \frac{\dot{\gamma}}{L} \vec{r}_{ij}^{\beta} \quad (1)$$

$$\vec{F}_{ij}^D(\vec{v}_{ij}^{\alpha}) := \vec{F}_{ij}^D(\vec{v}_{ij}^{*\alpha}). \quad (2)$$

Where $\vec{v}_{ij}^{*\alpha}$ is laminar flow velocity, \vec{v}_{ij}^{α} is the pairwise velocity parallel to the laminar flow field, \vec{r}_{ij}^{β} is the component of pairwise separation perpendicular to the flow field in the shear plane and L is the length of simulation box. The effect of this modification is to exempt the laminar flow profile from dissipative forces, while al-

TABLE II. Density of the metastable melt of *n*-eicosane at 1 atmospheric pressure as a function of temperature.

Temperature [K]	Density [g/cm^3]	Reference
250	0.836	*
255	0.833	**
260	0.830	**
265	0.828	*
270	0.825	**
275	0.822	**
280	0.819	*

* Densities taken from Yi et al.³⁷

** Densities calculated by linear interpolation using data from³⁷.

lowing dissipation to operate as normal on the flow field with laminar flow subtracted.

B. Nucleus formation

Fig. 4 shows the induction time as a function of shear rate at 250K. There are two regimes, one in which flow has no effect on the induction time, and one where the induction time decreases as a power law with the shear rate. This observation agrees with experimental results^{16,75}. The critical shear rate above which nucleation is accelerated, $\dot{\gamma}_c$, can be estimated from the intersection of the line (continuous) drawn through the induction time data at high shear rates and a horizontal line (dashed) at the value of the induction time under quiescent conditions ($\dot{\gamma} = 0$). At $\dot{\gamma} < \dot{\gamma}_c$ the nuclei are oriented in any random direction, while at $\dot{\gamma} > \dot{\gamma}_c$ the nuclei are oriented on average in the direction of flow, i.e. the stems are parallel to the flow field. In Fig. 5, we show the average tilt angle of the critical nucleus with respect to the flow field at different shear rates. With increasing shear rate the alignment becomes stronger. A similar observation has been reported for experiments on short polymer chains^{76,77}. In the inset of Fig. 4, the size of the critical nucleus is plotted against the shear rate: no effect of shear is evident.

Next we discuss the effect of temperature on the nucleation rate under shear flow. We carried out simulations at seven different temperatures ranging from 250K to 280K at a shear rate of $0.001\tau^{-1}$ ($0.95 \times 10^9\text{sec}^{-1}$). The integration timestep used in the simulations at 250K was 0.005τ . Fig. 6 shows the nucleation rate versus temperature. As expected, the nucleation rate decreases with increase in temperature. However, it increases only by a factor of 5 over the temperature range from 250K to 275K. The flow effects on the nucleation rates are stronger than the temperature effects – this observation has also been made in experiments^{16,75}. In the inset of Fig. 6, we show the critical nucleus size at different degrees of supercooling. The critical nucleus size depends only weakly on temperature.

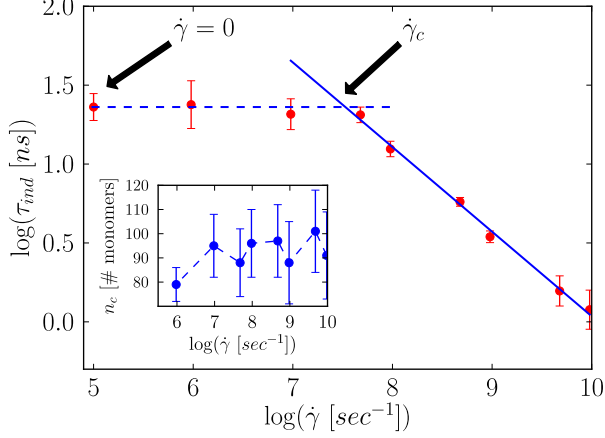


FIG. 4. Main panel: Induction time versus shear rate for C20 at 250K. Inset: size of critical nucleus versus logarithm of shear rate.

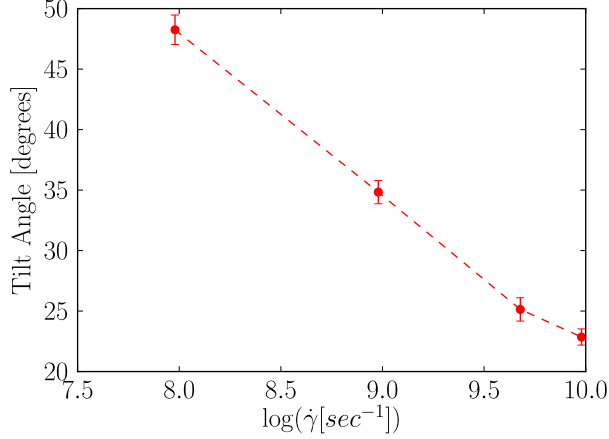


FIG. 5. C20: Average tilt angle between the critical nucleus and the flow direction versus the logarithm of the shear rate.

To study the nucleation mechanism we analyze 10 independent trajectories for every shear rate again in terms of the average radius of gyration R_g of all chains that are part of the nucleus at t_0 , the nematic order S_2 of these chains, the average volume V of the Voronoi cell associated to each particle that is part of the nucleus and its crystallinity order parameter. In Fig. 7 we show the relative variations of these quantities with respect to the values they had at $-100\Delta t$, $-70\Delta t$, $-35\Delta t$ and $-10\Delta t$ respectively, where $\Delta t = 10000\tau$, at shear rates $\dot{\gamma} = 0.00001\tau^{-1}$ ($0.95 \times 10^8 sec^{-1}$), $\dot{\gamma} = 0.0001\tau^{-1}$ ($0.95 \times 10^9 sec^{-1}$), $\dot{\gamma} = 0.001\tau^{-1}$ ($0.95 \times 10^9 sec^{-1}$) and $\dot{\gamma} = 0.01\tau^{-1}$ ($0.95 \times 10^{10} sec^{-1}$) respectively.

For the lowest shear rate, $\dot{\gamma} = 0.00001\tau^{-1}$, on approach to the formation of the critical nucleus at t_0 we observe first an increase in the global orientational order S_2 , then an increase in the radius of gyration and in the local den-

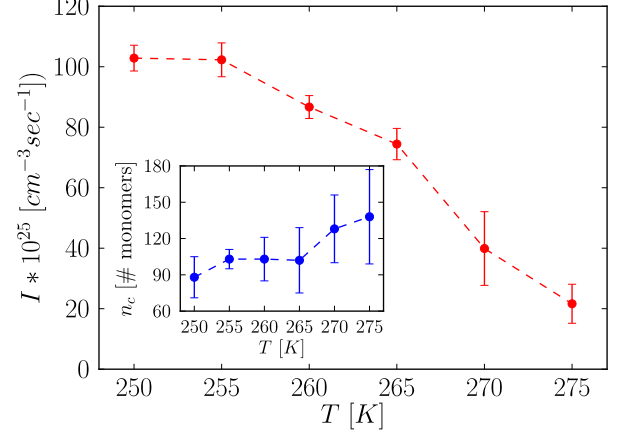


FIG. 6. Main panel: Nucleation rate versus temperature under shear flow for C20. Inset: size of the critical nucleus versus temperature.

sity, and finally local positional and orientational order are established. Thus the nucleation mechanism is the same as in the quiescent case⁴⁰: first the chains align, then they straighten.

At $\dot{\gamma} = 0.0001\tau^{-1}$ and at higher shear rates, we observe an increase in the global orientational order S_2 and simultaneously in the radius of gyration R_g . As expected^{13,78}, when shear is imposed on the system, the chains are straightened and oriented in the direction of flow. Thus alignment is enhanced, and the crystallization kinetics are accelerated.

We have shown that the flow field has an effect on the nucleation rate. In turn, the presence of nucleus should also have an effect on the flow field, because the mechanical properties of the crystalline state differ considerably from those of the melt. In fig. 8 we show the shear viscosity (measured using the instantaneous system average of the stress tensor) as a function of cluster size for a system consisting of 500 chains of C20, at 250K and at a shear rate of $0.001\tau^{-1}$. The black dots represent the simulation data points (which are subject to strong fluctuations due to the small system size), the red dashed line shows the size of the critical nucleus, the white line represents the mean value of the viscosity and the green envelop around the white line represents the standard deviation. We do not observe any change in the viscosity during the formation of the nucleus and growth up to cluster size of 450 monomers. Above this cluster size the scalar pressure started to decrease, because the phase transition was simulated in the NVT ensemble. We conclude that the nucleation events do not have an effect on the flow field, as the nuclei are small for the temperatures that we discuss here.

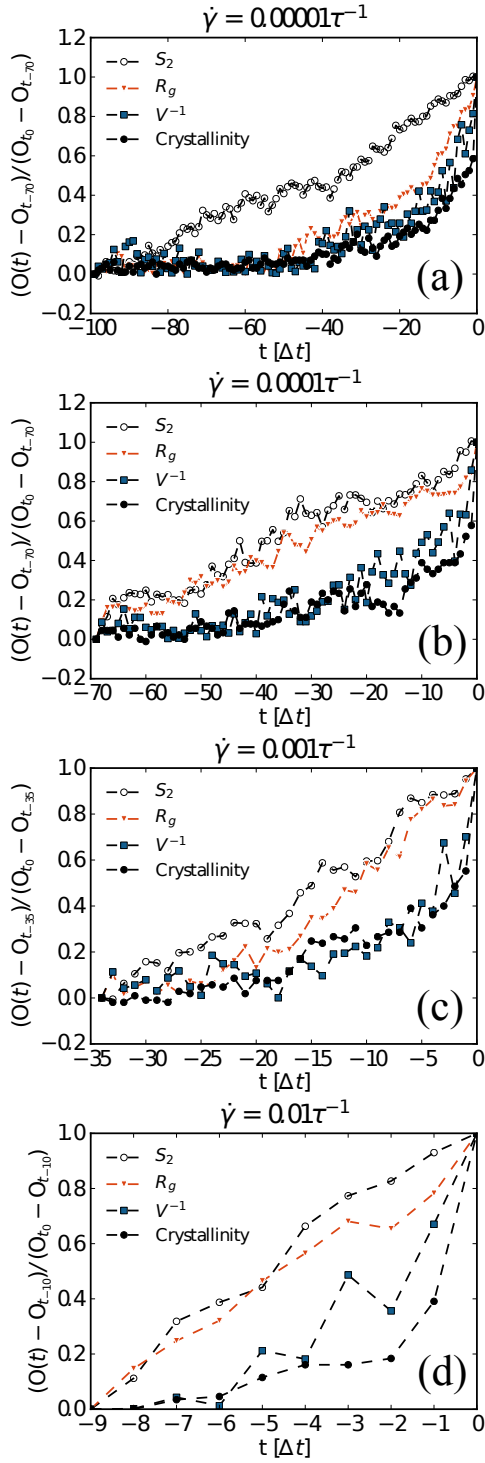


FIG. 7. C20 under shear: Relative variation of several observables (O) from the melt to the formation of a critical nucleus for the particles that are part of the critical nucleus at t_0 : nematic order S_2 (black, open circles), the radius of gyration R_g (red, triangles), the inverse of the Voronoi cell volume V (blue, squares) and the crystallinity order parameter (black, closed circles). (a) : $\dot{\gamma} = 0.00001\tau^{-1}$, (b) : $\dot{\gamma} = 0.0001\tau^{-1}$, (c) : $\dot{\gamma} = 0.001\tau^{-1}$, (d) : $\dot{\gamma} = 0.01\tau^{-1}$. The curves are averaged over 10 independent trajectories progressing backward in time from the nucleation time $t = t_0$ to $t = -100\Delta t$ at $\dot{\gamma} = 0.00001\tau^{-1}$, $t = -70\Delta t$ at $\dot{\gamma} = 0.0001\tau^{-1}$, $t = -35\Delta t$ at $\dot{\gamma} = 0.001\tau^{-1}$ and $t = -10\Delta t$ at $\dot{\gamma} = 0.01\tau^{-1}$ respectively. Here $\Delta t = 10000\tau$.

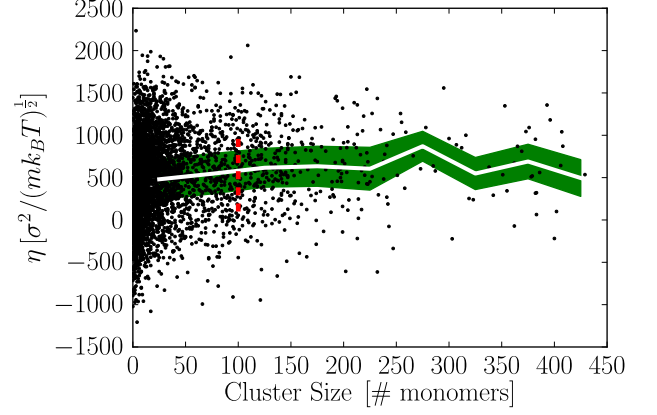


FIG. 8. C20: Shear viscosity as a function of cluster size. The black dots represent the simulation data points, the red dashed line shows the size of the critical nucleus, the white line represents the mean value of the viscosity and the green envelop around the white line represents standard deviation.

IV. C150 UNDER SHEAR

A. Simulation details

We performed simulations of 100 chains of C150. We equilibrated the system at 500K and then quenched it to 280K. All simulations were carried out under constant volume and controlled temperature conditions at a density of 0.89 g/cm^3 . We applied shear rates $\dot{\gamma}$ ranging from $0.0001\tau^{-1}$ to $0.005\tau^{-1}$ ($1.012 \times 10^8 \text{ sec}^{-1}$ to $5.06 \times 10^9 \text{ sec}^{-1}$).

B. Nucleus formation

In Fig. 9 we show the induction time versus the shear rate. The red circles represent the simulation data points and the blue curve is a fit. Again, the critical shear rate can be estimated as the intersection of the fitted line (continuous) at higher shear rate and a horizontal line (dashed) at the value of the induction time under quiescent conditions ($\dot{\gamma} = 0$). This data point $\dot{\gamma} = 0$ is taken from the Table I. In the inset of Fig. 9, the critical nucleus size versus shear rate is shown. It is constant within the error bars. Thus all results are qualitatively the same as those shown in Fig. 4 for C20.

We analyze 10 independent trajectories for every shear rate in terms of the order parameters that we introduced in the previous section. In Fig. 10 we show the relative variations of these quantities with respect to the values they had at $-300\Delta t$, $-140\Delta t$, $-70\Delta t$ and $-20\Delta t$ respectively, where $\Delta t = 5000\tau$ at shear rates $\dot{\gamma} = 0.0001\tau^{-1}$ ($1.012 \times 10^8 \text{ sec}^{-1}$), $\dot{\gamma} = 0.0005\tau^{-1}$ ($5.06 \times$

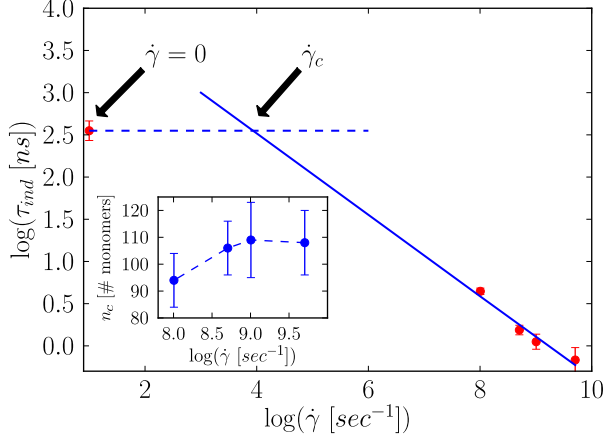


FIG. 9. Main panel: Induction time against shear rate for C150. Simulation data (red cricles) and fit (blue line). Inset: Size of the critical nucleus against log of shear rate.

10^8sec^{-1}), $\dot{\gamma} = 0.001\tau^{-1} (1.012 \times 10^9 \text{sec}^{-1})$ and $\dot{\gamma} = 0.005\tau^{-1} (5.06 \times 10^{10} \text{sec}^{-1})$ respectively.

For all shear rates, we observe first an increase in the nematic order S_2 , then an increase in the radius of gyration and in the local density, and finally the crystal structure with local order is formed. Thus we are in the regime of shear induced nucleation.

In Fig. 11, we show the tilt angle of the critical nucleus at different shear rates and we find the same trend as observed for C20.

In fig. 12 we show the shear viscosity as a function of cluster size at a shear rate of $0.001\tau^{-1}$. Again we do not observe any change in the viscosity during the formation of the nucleus and growth up to cluster size of 450 monomers.

V. CONCLUSIONS

We have simulated crystal nucleation from undercooled melts of short polymer chains under quiescent and shear conditions and analyzed the formation of the critical nucleus. For C150, which is longer than the entanglement length, we observe the same nucleation mechanism as for C20⁴⁰, which is shorter than the entanglement length: under quiescent conditions, first the chain segments align, then they straighten, and finally the cluster becomes denser and local positional and orientational order are established.

Under shear conditions, at low shear rates we observe the same mechanism as under quiescent conditions while at high shear rates the chains (or chain segments) align and straighten at the same time, then the local density increases and finally local positional and orientational order are established. We estimate the critical shear rates for

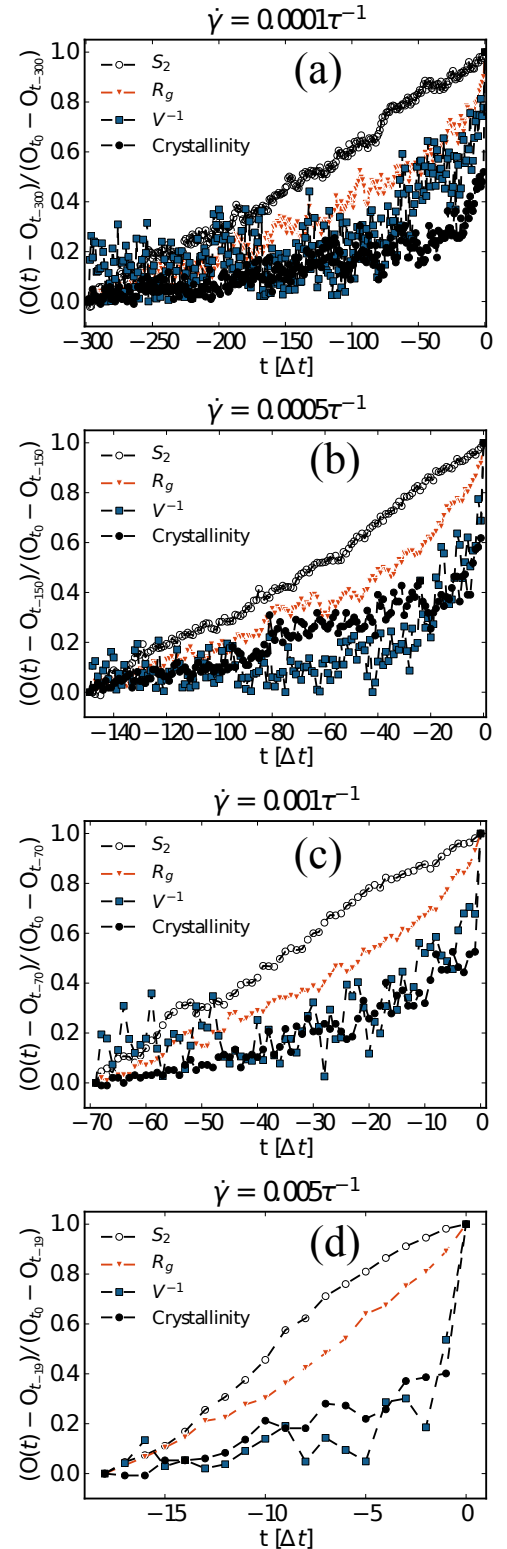


FIG. 10. C150: Relative variation of several observables (O) from the melt to the formation of a critical nucleus for the particles involved in the nucleus: the orientation order parameter S_2 (black, open circles), the radius of gyration R_g (red, triangles), the inverse of the Voronoi cell volume V (blue, squares) and the crystallinity order parameter (black, close circles). (a) : $\dot{\gamma} = 0.0001\tau^{-1}$, (b) : $\dot{\gamma} = 0.0005\tau^{-1}$, (c) : $\dot{\gamma} = 0.001\tau^{-1}$, (d) : $\dot{\gamma} = 0.005\tau^{-1}$. The curves are averaged over 10 independent trajectories progressing backward in time from the nucleation time $t = t_0$ to $t = -300\Delta t$ at $\dot{\gamma} = 0.0001\tau^{-1}$, $t = -140\Delta t$ at $\dot{\gamma} = 0.0005\tau^{-1}$, $t = -70\Delta t$ at $\dot{\gamma} = 0.001\tau^{-1}$ and $t = -20\Delta t$ at $\dot{\gamma} = 0.005\tau^{-1}$ respectively. Here $\Delta t = 5000\tau$.

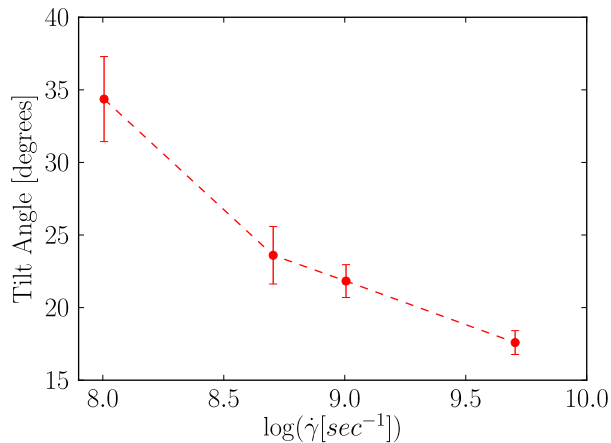


FIG. 11. C150: Tilt angle of nucleus versus shear rate.

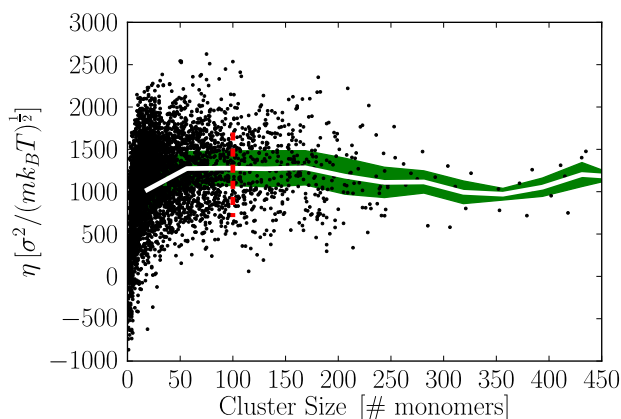


FIG. 12. C150: Shear viscosity as a function of cluster size. Shear viscosity as a function of cluster size. The black dots represent the simulation data points, the red dashed line shows the size of the critical nucleus, the white line represents the mean value of the viscosity and the green envelop around the white line represents standard deviation..

both systems(C20 & C150) and find power law behaviour between nucleation rate and shear rate as provided¹⁶.

ACKNOWLEDGMENTS

We thank Francesco Turci, Jens-Uwe Sommer, Roland Sanctuary, Jörg Baller and Carlo Di Giambattista for stimulating discussions. This project has been financially supported by the National Research Fund (FNR) within the CORE project Polyshear. Computer simulations presented in this paper were carried out using the HPC facility of the University of Luxembourg.

- ¹M. Muthukumar, "Nucleation in polymer crystallization," in *Advances in Chemical Physics* (John Wiley & Sons, Inc., 2004) pp. 1–63.
- ²M. Imai, K. Kaji, and T. Kanaya, *Macromolecules* **27**, 7103 (1994).
- ³K. T. S. Y. Imai M, Kaji K, *Physical Review B* **52**, 12696 (1995).
- ⁴T. A. Ezquerra, E. López-Cabarcos, B. S. Hsiao, and F. J. Baltà-Calleja, *Physical Review E* **54**, 989 (1996).
- ⁵A. Keller, M. Hikosaka, S. Rastogi, A. Toda, P. Barham, and G. Goldbeck-Wood, *Journal of Materials Science* **29**, 2579 (1994).
- ⁶M. T. K. K. K. T. Imai M, Mori K, *Polymer* **33**, 4451 (1992).
- ⁷G. Strobl, *The European Physical Journal E* **3**, 165 (2000).
- ⁸G. Strobl, *The European Physical Journal E* **18**, 295 (2005).
- ⁹G. Strobl, *Progress in Polymer Science* **31**, 398–442 (2006).
- ¹⁰T. Y. C. G. Strobl, *Eur. Phys. J. E* **23**, 55 (2007).
- ¹¹G. Strobl, *Reviews of Modern Physics* **81**, 1287 (2009).
- ¹²R. Somani, L. Yang, I. Sics, B. Hsiao, N. Pogodina, H. Winter, P. Agarwal, H. Fruitwala, and A. Tsou, *Macromolecular Symposia* **185**, 105 (2002).
- ¹³R. H. Somani, L. Yang, and B. S. Hsiao, *Physica A: Statistical Mechanics and its Applications* **304**, 145 (2002), scattering Studies of Mesoscopic Scale Structure and Dynamics in Soft Matter.
- ¹⁴F. M. Abuzaina, B. D. Fitz, S. Andjelić, and D. D. Jamiolkowski, *Polymer* **43**, 4699 (2002).
- ¹⁵G. F. D. Lellinger and I. Alig, *Polymer* **44**, 5759 (2003).
- ¹⁶S. Coppola, L. Balzano, E. Gioffredi, P. L. Maffettone, and N. Grizzuti, *Polymer* **45**, 3249 (2004).
- ¹⁷A. Elmoumni and H. Winter, *Rheologica Acta* **45**, 793 (2006).
- ¹⁸S. Acierno and N. Grizzuti, *International Journal of Material Forming* **1**, 583 (2008).
- ¹⁹R.-C. Zhang, A. Lu, and Z.-B. Xu, *Journal of Applied Polymer Science* **124**, 1562 (2012).
- ²⁰F. J. Custódio, R. J. Steenbakkers, P. D. Anderson, G. W. Peters, and H. E. Meijer, *Macromolecular Theory and Simulations* **18**, 469 (2009).
- ²¹J. van Meerveld, M. Hütter, and G. W. Peters, *Journal of Non-Newtonian Fluid Mechanics* **150**, 177 (2008).
- ²²H. Zuidema, G. W. Peters, and H. E. Meijer, *Macromolecular theory and simulations* **10**, 447 (2001).
- ²³S. E. M. Doi, *The Theory of Polymer Dynamics* (Oxford University Press, 1986).
- ²⁴T. Shimada, M. Doi, and K. Okano, *The Journal of Chemical Physics* **88**, 7181 (1988).
- ²⁵P. D. Olmsted, W. C. K. Poon, T. C. B. McLeish, N. J. Terrill and A. J. Ryan, *Physical Review Letters* **81**, 373 (1998).
- ²⁶B. M. Hongge Tan and D. Yan, *The Journal of Chemical Physics* **119**, 2886 (2003).
- ²⁷K. Kaji, "Handbook of thermoplastic polyesters: Homopolymers, copolymers, blends, and composites," in *Handbook of Thermoplastic Polyesters* (Wiley-VCH Verlag GmbH & Co. KGaA, 2005) Chap. Structure Formation in PET during the Induction Period of Crystallization, pp. 225–251.
- ²⁸R. S. Graham, A. E. Likhtman, T. C. B. McLeish, and S. T. Milner, *Journal of Rheology* (1978-present) **47**, 1171 (2003).
- ²⁹R. S. Graham and P. D. Olmsted, *Physical Review Letters* **103**, 115702 (2009).
- ³⁰R. S. Graham and P. D. Olmsted, *Faraday discussions* **144**, 71 (2010).
- ³¹K. Jolley and R. S. Graham, *The Journal of Chemical Physics* **134**, 164901 (2011).
- ³²K. Esselink, P. A. J. Hilbers, and B. W. H. van Beest, *The Journal of Chemical Physics* **101**, 9033 (1994).
- ³³H. Takeuchi, *The Journal of Chemical Physics* **109**, 5614 (1998).
- ³⁴S. Fujiwara and T. Sato, *Physical Review Letters* **80**, 991 (1998).
- ³⁵S. Fujiwara and T. Sato, *The Journal of Chemical Physics* **110**, 9757 (1999).
- ³⁶P. Yi and G. C. Rutledge, *The Journal of Chemical Physics* **131**, 1 (2009).
- ³⁷P. Yi and G. C. Rutledge, *The Journal of Chemical Physics* **135**, 11 (2011).

- ³⁸P. Yi, C. R. Locker, and G. C. Rutledge, *Macromolecules* **46**, 4723 (2013).
- ³⁹H. Zerbe, J. Mittal, and A. J. McHugh, *Macromolecules* **46**, 9151 (2013).
- ⁴⁰M. Anwar, F. Turci, and T. Schilling, *The Journal of Chemical Physics* **139**, 214904 (2013).
- ⁴¹T. Yamamoto, *The Journal of Chemical Physics* **139**, 054903 (2013).
- ⁴²T. Yamamoto, *The Journal of Chemical Physics* **133**, 034904 (2010).
- ⁴³T. Yamamoto, *The Journal of Chemical Physics* **129**, 184903 (2008).
- ⁴⁴T. Yamamoto, *Polymer* **45**, 1357 (2004), modeling of Chain Conformations and Spatial Configurations.
- ⁴⁵T. Yamamoto, *The Journal of Chemical Physics* **109**, 4638 (1998).
- ⁴⁶C. Luo and J.-U. Sommer, *Macromolecules* **44**, 1523 (2011).
- ⁴⁷C. Luo and J.-U. Sommer, *Physical Review Letters* **102**, 147801 (2009).
- ⁴⁸P. Welch and M. Muthukumar, *Physical Review Letters* **87**, 218302 (2001).
- ⁴⁹H. Meyer and F. Müller-Plathe, *The Journal of Chemical Physics* **115**, 7807 (2001).
- ⁵⁰J.-U. Sommer and G. Reiter, *The Journal of Chemical Physics* **112**, 4384 (2000).
- ⁵¹N. Waheed, M. S. Lavine, and G. C. Rutledge, *The Journal of Chemical Physics* **116**, 2301 (2002).
- ⁵²M. Muthukumar, "Modeling polymer crystallization," in *Interphases and Mesophases in Polymer Crystallization III*, Advances in Polymer Science, Vol. 191, edited by G. Allegra (Springer Berlin Heidelberg, 2005) pp. 241–274.
- ⁵³M. Muthukumar, *Phil. Trans. Roy. Soc. A* **361**, 539 (2003).
- ⁵⁴M. Muthukumar, *The European Physical Journal E* **3**, 199 (2000).
- ⁵⁵A. Koyama, T. Yamamoto, K. Fukao, and Y. Miyamoto, *Physical Review E* **65**, 050801 (2002).
- ⁵⁶A. Koyama, T. Yamamoto, K. Fukao, and Y. Miyamoto, *Journal of Macromolecular Science, Part B* **42**, 821 (2003).
- ⁵⁷M. S. Lavine, N. Waheed, and G. C. Rutledge, *Polymer* **44**, 1771 (2003).
- ⁵⁸M. J. Ko, N. Waheed, M. S. Lavine, and G. C. Rutledge, *The Journal of Chemical Physics* **121**, 2823 (2004).
- ⁵⁹T. C. Ionescu, C. Baig, B. J. Edwards, D. J. Keffer, and A. Habenschuss, *Physical Review Letters* **96**, 037802 (2006).
- ⁶⁰A. Jabbarzadeh and R. Tanner, *Journal of Non-Newtonian Fluid Mechanics* **160**, 11 (2009), complex flows of complex fluids.
- ⁶¹I. Dukovski and M. Muthukumar, *The Journal of Chemical Physics* **118**, 6648 (2003).
- ⁶²C. Baig and B. J. Edwards, *Journal of Non-Newtonian Fluid Mechanics* **165**, 992 (2010), proceedings of the 5th International Workshop on Non-Equilibrium Thermodynamics 2009.
- ⁶³C. Baig and B. J. Edwards, *EPL* **89**, 36003 (2010).
- ⁶⁴W. Paul, D. Y. Yoon, and G. D. Smith, *The Journal of Chemical Physics* **103**, 1702 (1995).
- ⁶⁵H. J. Limbach, A. Arnold, B. A. Mann, and C. Holm, *Computer Physics Communications* **174**, 704 (2006).
- ⁶⁶J. Qin and S. T. Milner, *Soft Matter* **7**, 10676 (2011).
- ⁶⁷R. S. Hoy, K. Foteinopoulou, and M. Kröger, *Physical Review E* **80**, 031803 (2009).
- ⁶⁸G. Subramanian and S. Shanbhag, *The Journal of Chemical Physics* **129**, 144904 (2008).
- ⁶⁹M. Tanaka, K. Iwata, and N. Kuzuu, *Computational and Theoretical Polymer Science* **10**, 299 (2000).
- ⁷⁰A. Kolb and B. Dünweg, *Journal of Chemical Physics* **111**, 4453 (1999).
- ⁷¹J. Wedekind, R. Strey, and D. Reguera, *The Journal of Chemical Physics* **126**, 134103 (2007).
- ⁷²C. H. Rycroft, *Chaos* **19**, 041111 (2009).
- ⁷³T. Soddemann, B. Dünweg, and K. Kremer, *Physical Review-Physical Review Letters* **E 68**, 046702 (2003).
- ⁷⁴A. Chatterjee, *Molecular Simulation* **33**, 1233 (2007).
- ⁷⁵M. Derakhshandeh and S. Hatzikiriakos, *Rheologica Acta* **51**, 315 (2012).
- ⁷⁶E. Manias, *A computer simulation study Nanorheology of strongly confined molecular fluids*, Ph.D. thesis, State University of Groningen The Netherlands (1995).
- ⁷⁷G. H. Peters and D. J. Tildesley, *Physical Review E* **52**, 1882 (1995).
- ⁷⁸R. Graham, *Journal of Engineering Mathematics* **71**, 237 (2011).